Supporting Information for the paper:

Molecule-like and Lattice Vibrations in Metal Clusters

Krishnadas Kumaranchira Ramankutty,* Huayan Yang, Ani Baghdasaryan,
Jeremie Teyssier, Valentin Paul Nicu* and Thomas Buergi*

1. General Experimental parameters used for ESI MS measurements

The sample solubilized in dichloromethane was analyzed by nano-electrospray high resolution mass spectrometry (nano-ESI-HRMS) with the following settings:

- QSTAR Pulsar (AB Sciex)

- nano-ESI voltage = -2600 kV and -2200 kV (negative),

- Curtain gas (N2) = 25 psi

- Declustering and focusing lenses: DP = -50 V, DP2 = -15 V, FP = -120 V

- Mass range: m/z 100 – 12'000 (accumulation time = 1s) with external TOF calibration (Agilent)

- Bin = 1 (automatic signal smoothing)

- Data processing software: PeakView 2.2 (AB Sciex)

External TOF calibration was performed prior to sample analysis up to m/z 2834. Mass accuracy above this value cannot be guaranteed.

Supporting Information 1
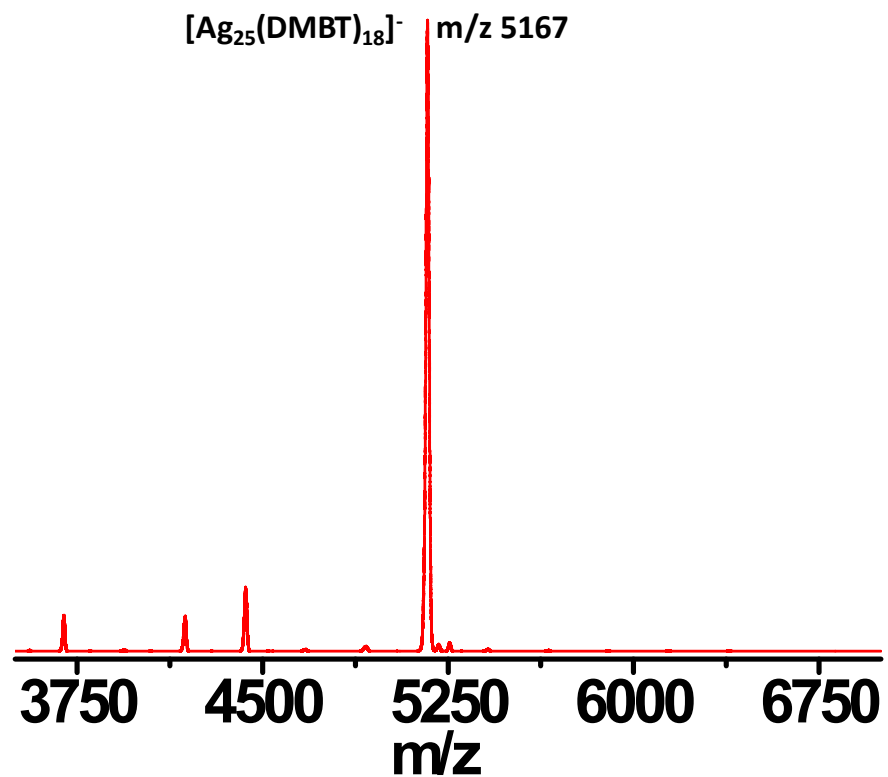
Figure S1. Negative ion mode ESI mass spectrum of $[Ag_{25}(DMBT)_{18}][PPh_4]$. The bands in the lower m/z region are due to the fragments due to the sequential loss of the Ag-DMBT fragments from the molecular ion.

Supporting Information 2
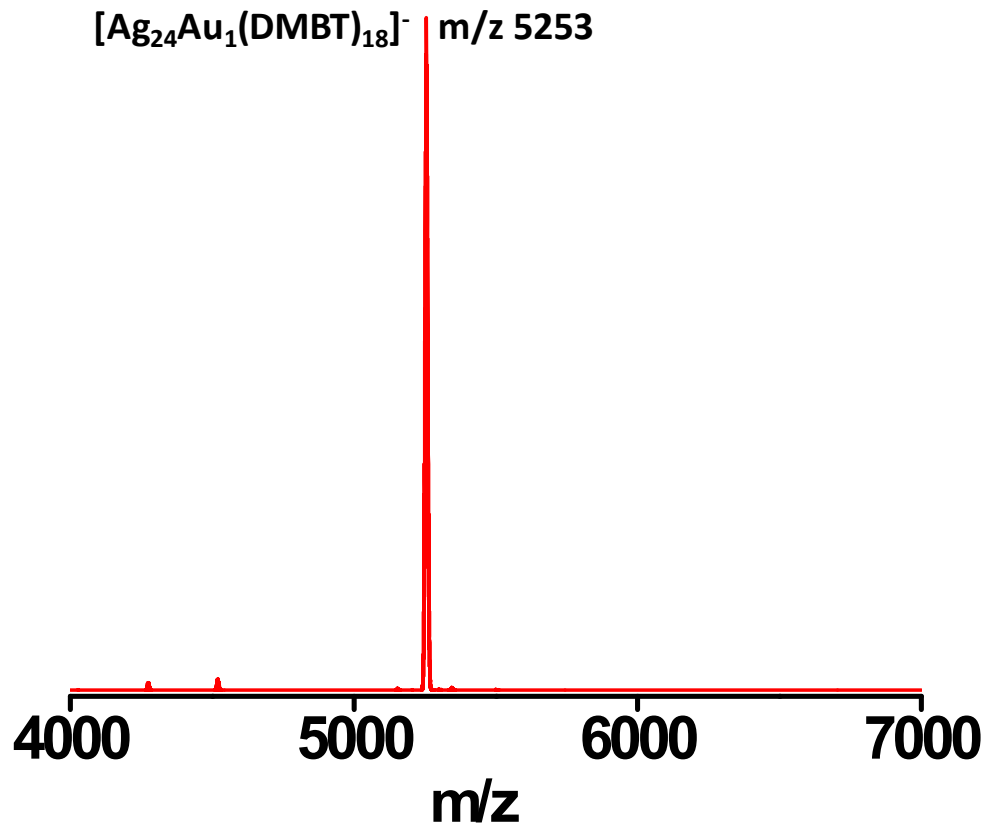
Figure S2. Negative ion mode ESI mass spectrum of $[Ag_{24}Au_1(DMBT)_{18}][PPh_4]$. The bands in the lower m/z region are due to the fragments due to the sequential loss of the Ag-DMBT fragments from the molecular ion.

Supporting Information 3

$[Au_{25}(PET)_{18}]^+$ m/z 7391

-(Au-PET) -(Au-PET)-(Au-PET) -(Au-PET)

6000   6750   7500   8250

m/z
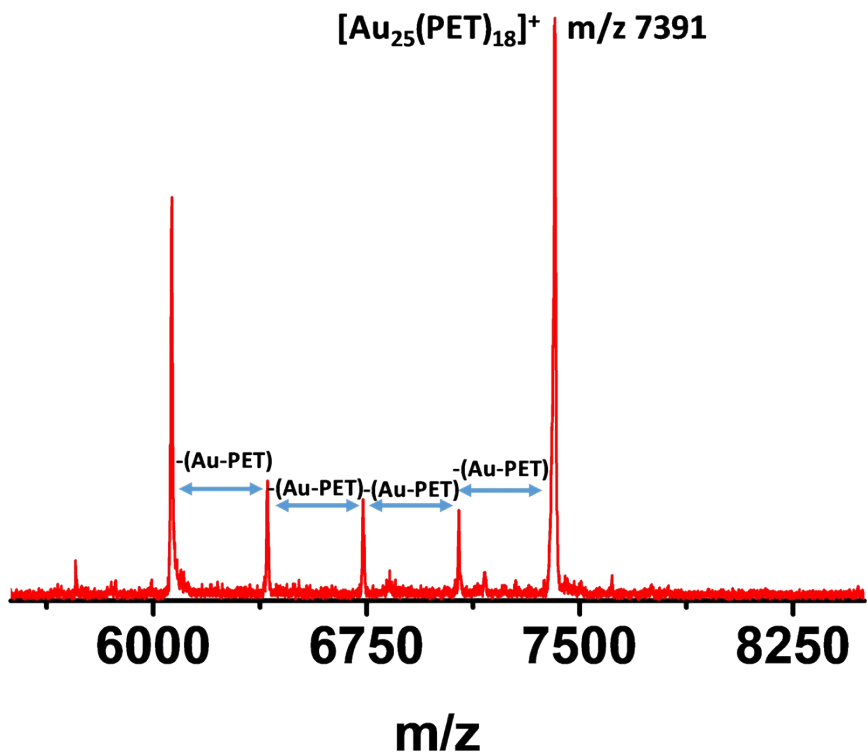
Figure S3. Positive ion mode MALDI mass spectrum of $[Au_{25}(PET)_{18}]$. The bands in the lower m/z region are due to the fragments due to the sequential loss of the Au-PET fragments from the molecular ion, as labeled in the figure.
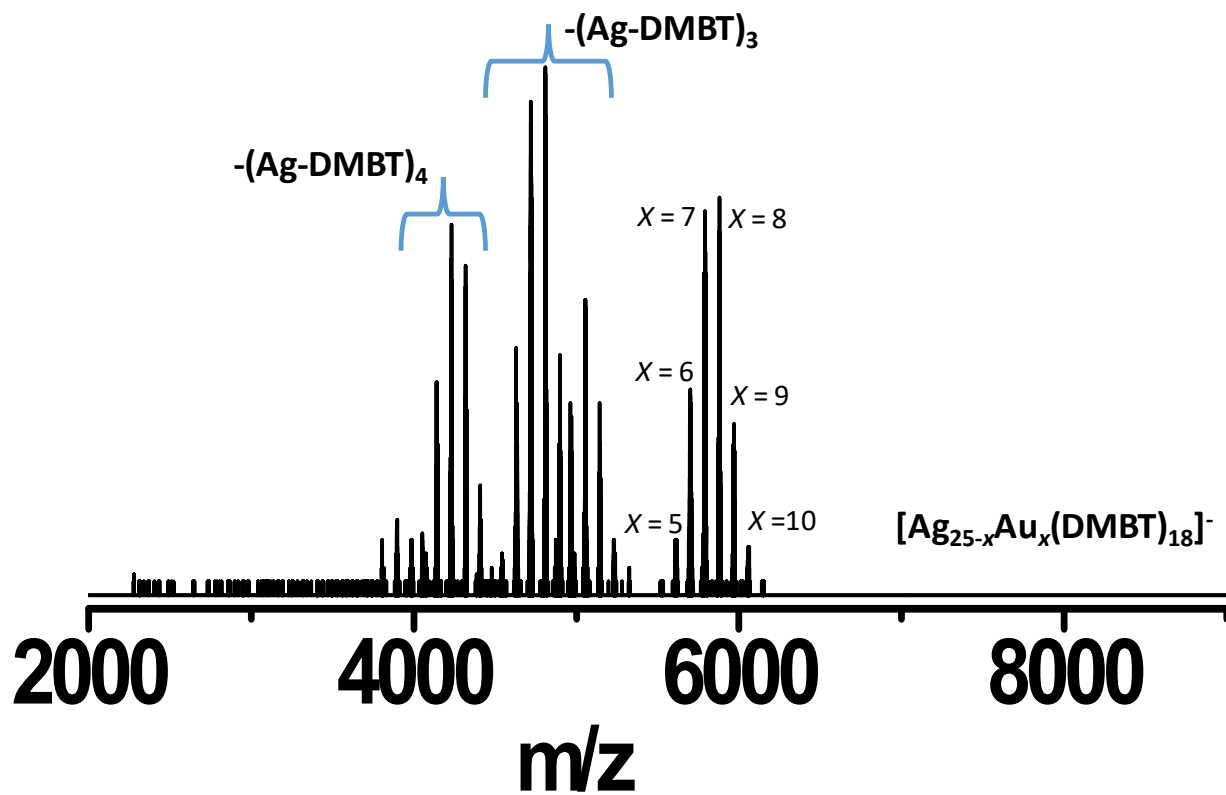
Figure S4. Negative ion mode MALDI mass spectrum of $[Ag_{25-x}Au_x(DMBT)_{18}]$ alloy I.

Supporting Information 5
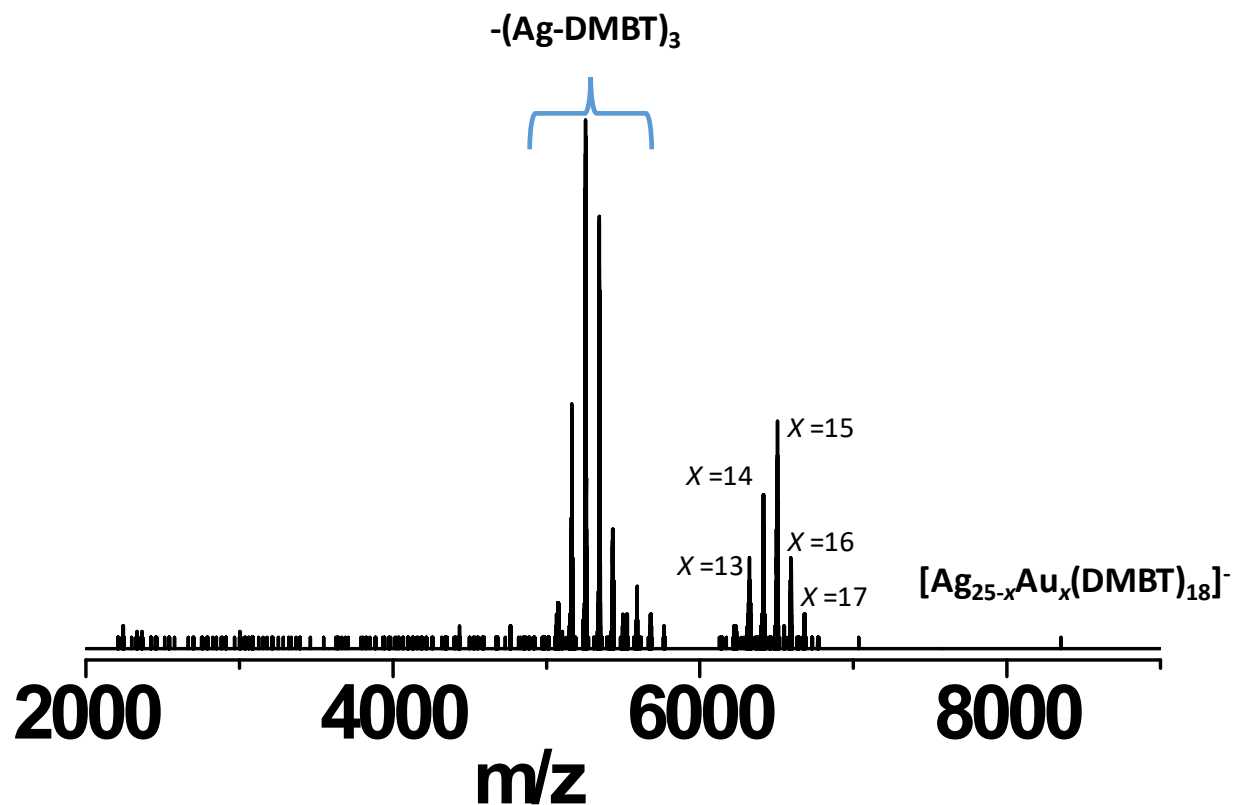
Figure S5. Negative ion mode MALDI mass spectrum of $[Ag_{25-x}Au_x(DMBT)_{18}]$ alloy II.
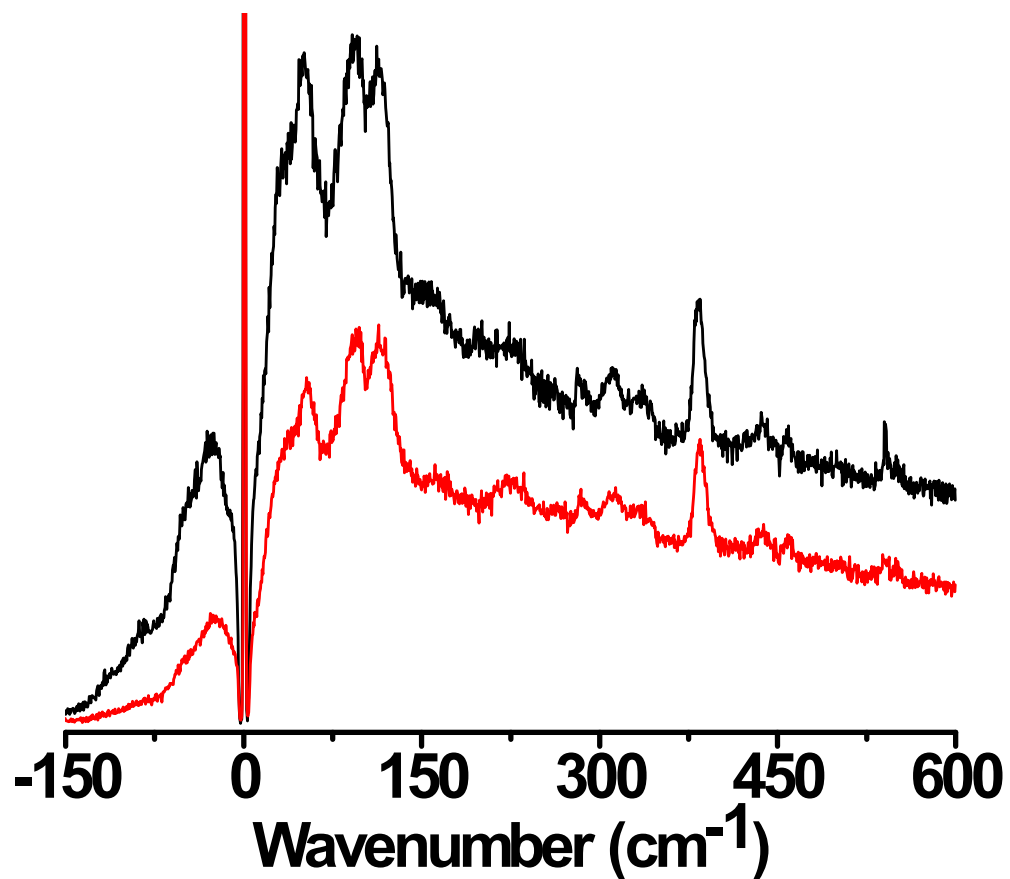
Figure S6. Raman spectra of [Ag$_{25}$(DMBT)$_{18}$][PPh$_4$] (black trace) and [Ag$_{24}$Au$_1$(DMBT)$_{18}$][PPh$_4$] (red trace).

Supporting Information 7
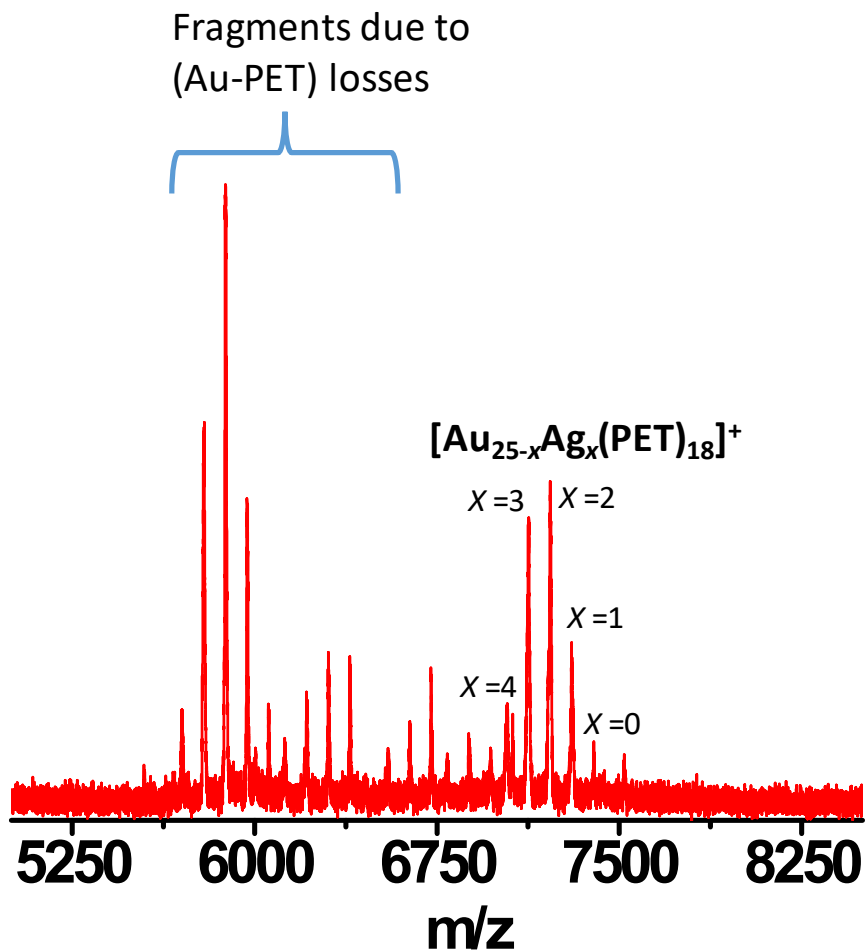
Figure S7. Positive ion mode MALDI mass spectrum of $[Au_{25-x}Ag_x(PET)_{18}]$.
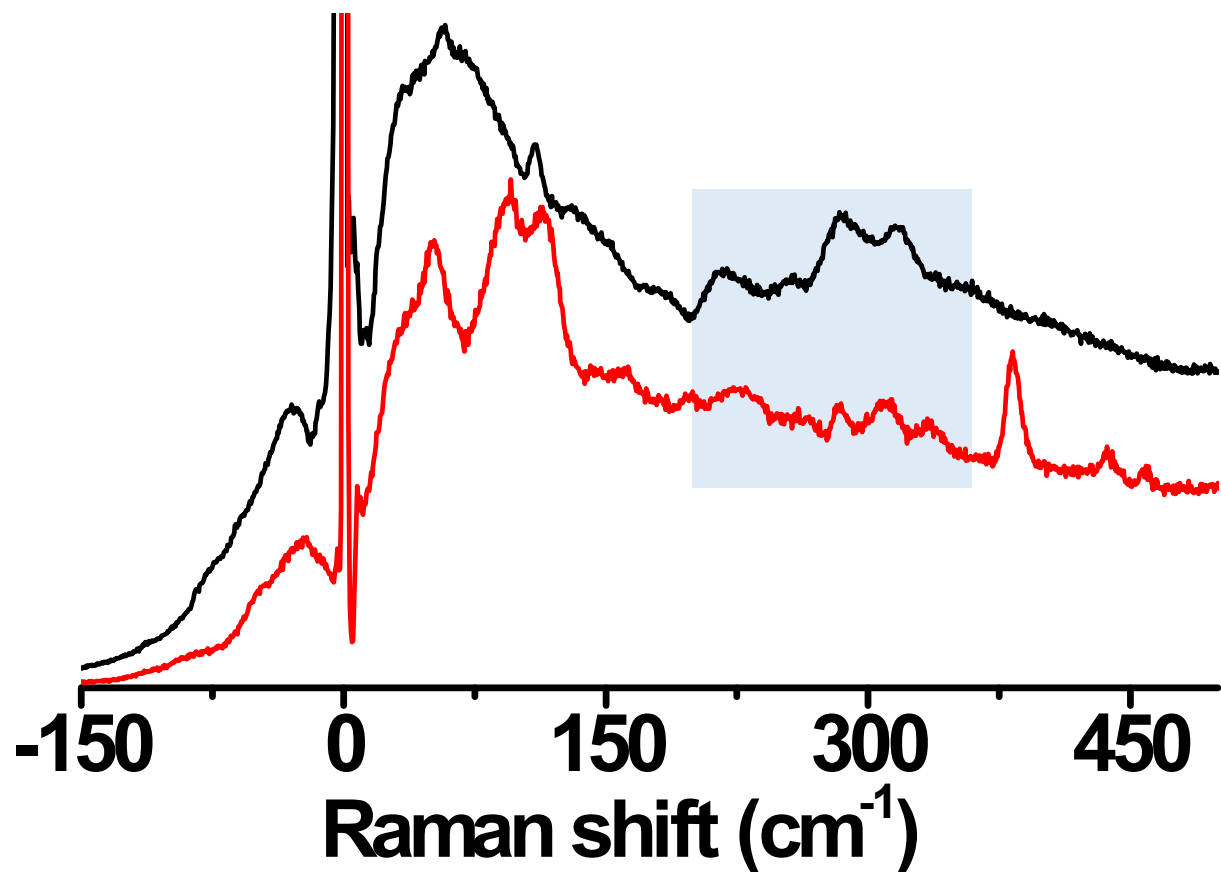
Figure S8. A comparison of the Raman spectrum of $Au_{25}(PET)_{18}$ (black trace) and $Ag_{25}(DMBT)_{18}$ (red trace). The region highlighted in blue shows the similarity of the high-frequency Raman bands of these two clusters.

Supporting Information 9
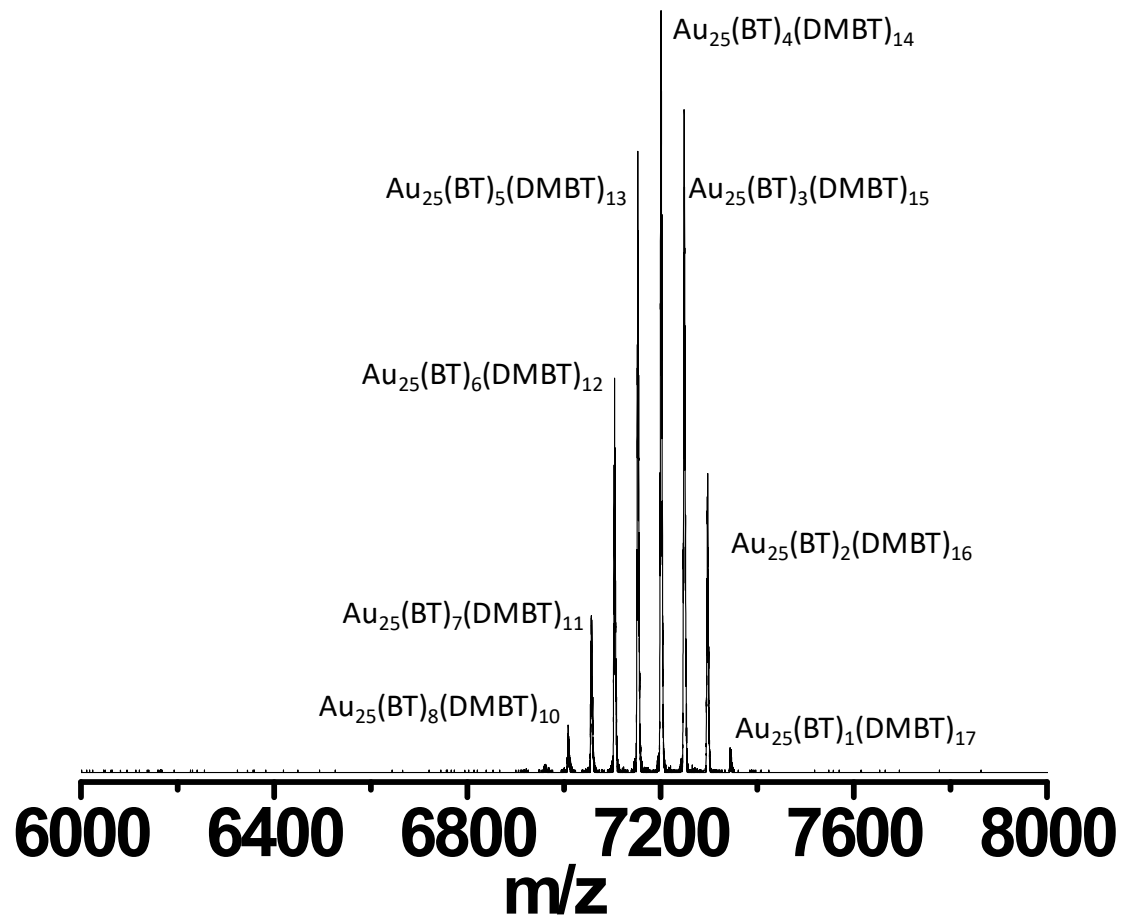
Figure S9. Positive ion mode ESI mass spectra of $Au_{25}(BT)_{18-x}(DMBT)_x$ clusters.
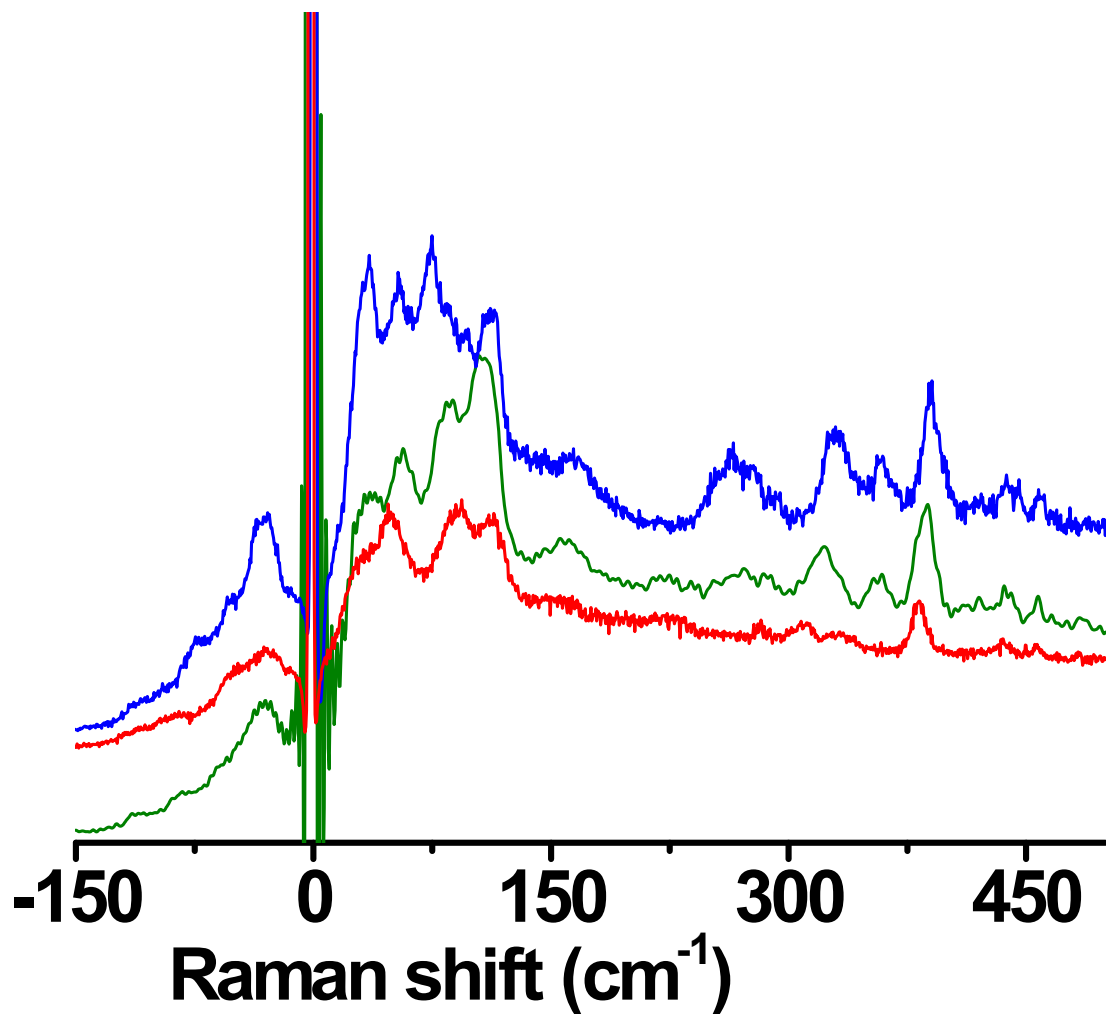
Figure S10. Raman spectra of $[Ag_{25}(DMBT)_{18}][PPh_4]$ (red trace), $Ag_{25-x}Au_x$-Alloy II (green trace) and $Au_{25}(BT)_{18-x}(DMBT)_x$ (blue trace).

Supporting Information 11

Normal mode analysis

The similarity/differences between the normal modes computed for the Au_{25}, Ag_{25} and $Ag_{24}Au$ clusters were assessed by calculating normal mode overlaps, i.e., scalar products between the normalised nuclear displacement vectors. In addition, the localisation of the mode motion on the inner-cores (i.e., Au_{13}, Ag_{13} and $Ag_{12}Au_1$), the $(Au_2S_3)_6$ ligand binding motifs and the remaining C and H atoms was computed using the following formula:

$$L(j,X) = \frac{\sum_{i=1,N^X} S_i^2(j)}{\sum_{i=1,N^{tot}} S_i^2(j)}$$

where $L(j,X)$ is the localisation of the motion associated with normal mode j on the molecular fragment X, $S_i^2(j)$ is the square of the nuclear displacement vector S associated with the ith atom and the jth normal mode, N^X is the number of atoms in fragment X and N^{tot} is the total number of atoms in the molecule.

Three different fragments have been considered when computing the localisation of the normal mode motion. Fragment one (F1) represents the Au_{13}, Ag_{13} and $Ag_{12}Au$ inner- cores, fragment two (F2) the $(Au_2S_3)_6$ ligand binding motifs and fragment three (F3) the remaining C and H atoms. Further, there are two important points that need to be made about the localisation of the normal mode motion. First, the localisation of the normal mode motion on fragment F3 will be significantly larger than on the other two fragments combined. This happens because the C and H atoms are lighter and more numerous than the Au/Ag and S atoms. Second, the nuclear displacement vectors associated with the C and H atoms have little relevance for the interpretation of the experimental spectra. This is because the CH_3 group is not only significantly lighter than the DMBT group it has substituted, but it also has a very different geometry. Consequently, when assigning the character of the Raman bands, we only take into account the localisation of the modes on the fragments F1 and F2. For this reason, there are two normal mode overlap values listed in Tables I, II and II (i.e., O1 is obtain by considering the nuclear displacement vectors of all atoms in the nanoclusters, while the O2 is calculated without the nuclear displacement vectors of the C and H atoms.)

Table I lists the results obtained when comparing the modes of the Au_{25} and Ag_{25} clusters. The analysis was performed for all Au_{25} modes with a significant Raman intensity. Furthermore, only the Ag_{25} modes that exhibits an overlap larger than 0.6 with the Au_{25} modes have been listed in Table I. Tables II and III list the results obtained when comparing the Ag_{25} and $Ag_{24}Au_1$ modes

with significant Raman intensities. To illustrate the meaning of the values taken by a given normal mode overlap, in Figure S12 we considered one Ag_{25} mode from each of the six Ag_{25} bands (i.e., the most intense mode) together with their corresponding $Ag_{24}Au_1$ modes and superimposed their nuclear displacement vectors. An overlap of 0.99 (e.g. modes 43 in Figure S12), means that the two modes are 98% ($0.98 = 0.99^2$) similar. In turn, this implies that all nuclear displacement vectors have very similar directions and magnitudes. Similarly, an overlap of 0.79 (e.g. modes 77 in Figure S12), means that the two modes are only 62% ($0.62 = 0.79^2$) similar. While the two modes can still be considered as similar, their nuclear displacement vectors exhibit clear difference both in direction and magnitude.

Supporting Information 12

mode 16 of Ag$_{25}$S$_{18}$ vs. mode 16 of Ag$_{24}$Au$_1$S$_{18}$	mode 43 of Ag$_{25}$S$_{18}$ vs. mode 43 of Ag$_{24}$Au$_1$S$_{18}$	mode 70 of Ag$_{25}$S$_{18}$ vs. mode 70 of Ag$_{24}$Au$_1$S$_{18}$
$O_2 = 0.97$	$O_2 = 0.99$	$O_2 = 0.92$
mode 77 of Ag$_{25}$S$_{18}$ vs. mode 78 of Ag$_{24}$Au$_1$S$_{18}$	mode 97 of Ag$_{25}$S$_{18}$ vs. mode 97 of Ag$_{24}$Au$_1$S$_{18}$	mode 106 of Ag$_{25}$S$_{18}$ vs. mode 106 of Ag$_{24}$Au$_1$S$_{18}$
$O_2 = 0.79$	$O_2 = 0.84$	$O_2 = 0.95$
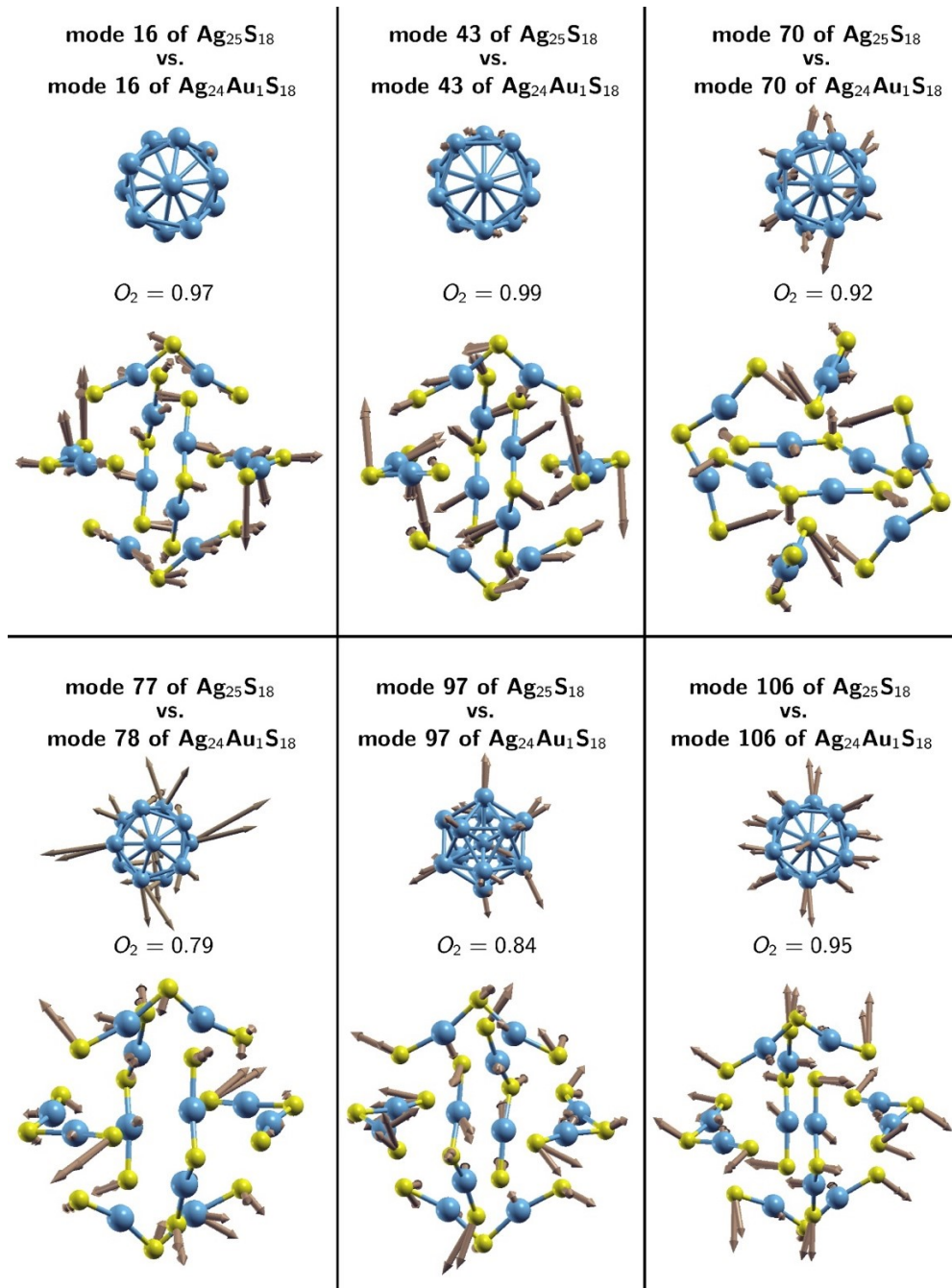
Figure S11. Overlaps between the nuclear displacement vectors of the Ag$_{25}$ and Ag$_{24}$Au$_1$ clusters. The O2 normal mode overlaps were computed using only the nuclear displacement vectors of the atoms in the Ag$_{25}$S$_{18}$ and Ag$_{24}$Au$_1$S$_{18}$ fragments.

Supporting Information 13

Cluster	NM	Freq.	Raman	NM Localisation			NM overlap		Band
				F1	F2	F3	O_1	O_2	
Au_{25}	11	22.4	2.401	3.0	16.1	80.8			
Au_{25}	14	25.0	2.528	7.3	19.3	73.5			A_1
Ag_{25}	7	22.8	2.776	1.6	15.4	83.0	0.64	0.47	
Au_{25}	16	25.5	2.121	4.3	17.2	78.5			
Au_{25}	19	28.0	2.772	4.2	27.0	68.8			
Au_{25}	21	28.6	3.458	4.3	25.3	70.4			
Au_{25}	22	28.7	2.137	5.1	25.4	69.5			
Ag_{25}	14	31.7	5.912	3.2	28.4	68.5	0.45	0.64	
Au_{25}	24	30.2	1.927	5.1	21.5	73.4			
Ag_{25}	7	22.8	2.776	1.6	15.4	83.0	-0.68	0.41	
Au_{25}	44	47.4	2.305	4.1	12.2	83.6			
Au_{25}	46	48.4	4.156	2.7	9.7	87.6			shoulder
Au_{25}	48	51.5	3.942	17.3	16.9	65.8			A_2
Ag_{25}	68	77.8	8.901	11.2	13.3	75.5	-0.42	-0.64	
Au_{25}	54	57.2	4.520	2.8	9.2	88.0			
Ag_{25}	49	57.9	1.697	2.8	12.9	84.4	-0.77	-0.64	A_2
Au_{25}	55	57.5	8.036	13.6	20.1	66.4			
Au_{25}	58	60.0	5.761	12.1	19.0	69.0			
Au_{25}	59	60.5	2.997	10.3	17.0	72.6			
Au_{25}	61	61.2	5.926	12.3	18.8	68.9			
Au_{25}	64	62.9	4.616	5.6	22.3	72.1			
Au_{25}	65	63.8	5.055	5.8	24.8	69.4			
Au_{25}	67	66.9	6.488	5.3	13.3	81.3			
Ag_{25}	52	62.9	6.458	5.2	11.1	83.7	-0.77	-0.17	
Ag_{25}	54	64.4	1.155	7.1	9.4	83.5	0.64	0.36	
Au_{25}	68	67.6	4.268	3.9	12.5	83.6			
Ag_{25}	52	62.9	6.458	5.2	11.1	83.7	-0.72	-0.54	
Au_{25}	83	100.7	7.330	10.0	12.7	77.4			
Au_{25}	84	104.6	26.793	8.5	11.4	80.1			A_3
Ag_{25}	106	130.1	18.532	4.0	6.9	89.1	0.28	-0.69	

Table S1. Comparison of the nuclear displacement vectors of the Au25 and Ag25 clusters. Only the modes with significant Raman intensities were considered. All atoms were considered when computing the $O1$ overlap. For $=O2$, the C and H atoms were neglected. Units: Freq (cm^{-1}), Raman (Ang^4/amu).

Cluster	NM	Freq.	Raman	NM Localisation			NM overlap		Band
				F1	F2	F3	O_1	O_2	
Ag_{25}	13	31.1	5.739	3.6	28.3	68.1			
$Ag_{24}Au$	13	31.5	5.251	3.5	28.6	67.9	0.99	0.99	C_1
Ag_{25}	14	31.7	5.912	3.2	28.4	68.5			
$Ag_{24}Au$	14	32.1	1.901	5.2	21.0	73.8	0.62	0.69	
$Ag_{24}Au$	15	32.2	4.265	4.3	24.9	70.8	0.51	0.75	
Ag_{25}	16	32.4	5.793	2.2	20.2	77.6			
$Ag_{24}Au$	16	33.0	5.979	2.1	20.2	77.7	0.99	0.97	
Ag_{25}	19	35.5	3.288	2.3	25.4	72.3			
$Ag_{24}Au$	19	35.8	2.452	2.7	24.9	72.4	0.99	1.00	
Ag_{25}	20	36.3	4.388	2.2	24.7	73.1			
$Ag_{24}Au$	20	37.0	4.095	1.9	25.3	72.7	0.99	0.99	
Ag_{25}	21	37.2	2.427	1.6	22.6	75.8			
$Ag_{24}Au$	21	37.4	2.248	1.6	22.4	76.1	0.99	0.99	
Ag_{25}	32	45.2	2.168	7.8	13.4	78.8			
$Ag_{24}Au$	32	44.9	2.420	7.5	12.0	80.4	-0.97	-0.96	C_2
Ag_{25}	33	45.7	3.491	4.8	16.7	78.5			
$Ag_{24}Au$	34	45.7	2.381	5.4	19.3	75.3	0.89	0.85	
Ag_{25}	38	47.9	3.053	7.5	20.9	71.6			
$Ag_{24}Au$	38	47.6	2.135	8.8	19.0	72.2	0.88	0.88	
Ag_{25}	39	48.3	2.809	5.8	21.2	73.0			
$Ag_{24}Au$	39	48.6	3.515	5.9	22.8	71.3	0.91	0.91	
Ag_{25}	40	49.6	2.990	8.2	22.0	69.8			
$Ag_{24}Au$	40	50.0	3.025	6.4	21.1	72.6	0.93	0.95	
Ag_{25}	43	51.3	4.056	2.8	16.0	81.3			
$Ag_{24}Au$	43	51.7	4.263	2.4	16.3	81.3	0.99	0.99	
Ag_{25}	52	62.9	6.458	5.2	11.1	83.7			
$Ag_{24}Au$	52	63.1	5.629	5.0	11.0	83.9	-0.99	-0.99	C_3
Ag_{25}	57	66.9	5.333	5.7	11.3	82.9			
$Ag_{24}Au$	57	67.5	3.786	5.9	11.3	82.7	-0.94	-0.94	
Ag_{25}	59	68.6	3.621	6.5	9.7	83.8			
$Ag_{24}Au$	59	69.2	3.786	5.8	9.6	84.6	0.97	0.96	
Ag_{25}	60	69.8	6.092	11.8	11.5	76.7			
$Ag_{24}Au$	60	70.5	4.996	12.3	10.3	77.4	0.96	0.96	
Ag_{25}	61	71.4	6.080	11.4	14.0	74.6			
$Ag_{24}Au$	62	72.3	5.857	12.8	13.5	73.7	-0.56	-0.79	
$Ag_{24}Au$	63	73.5	9.357	9.3	12.1	78.6	0.75	0.54	
Ag_{25}	63	72.4	8.541	11.8	14.2	74.0			
$Ag_{24}Au$	63	73.5	9.357	9.3	12.1	78.6	-0.82	-0.77	
Ag_{25}	64	74.8	4.820	7.1	12.0	80.9			
$Ag_{24}Au$	64	75.6	9.671	7.8	12.1	80.1	0.95	0.94	
Ag_{25}	65	75.1	9.617	10.6	12.4	77.0			
$Ag_{24}Au$	65	76.3	8.644	9.9	12.4	77.7	-0.94	-0.95	

Table S2. Comparison of the nuclear displacement vectors of the Ag_{25} and $Ag_{24}Au$ clusters. Only the modes with significant Raman intensities were considered. All atoms were considered when computing the $O1$ overlap. For $=O2$, the C and H atoms were neglected. Units: Freq (cm^{-1}), Raman (Ang^4/amu).

Supporting Information 15

Cluster	NM	Freq.	Raman	NM Localisation			NM overlap		Band
				F1	F2	F3	O_1	O_2	
Ag_{25}	68	77.8	8.901	11.2	13.3	75.5			
$Ag_{24}Au$	69	78.7	5.774	15.2	14.2	70.6	0.74	0.76	C_3
Ag_{25}	70	79.0	11.005	9.2	12.7	78.1			
$Ag_{24}Au$	70	79.2	11.196	10.0	12.8	77.3	0.95	0.92	
Ag_{25}	74	87.1	4.646	28.6	15.5	55.9			
$Ag_{24}Au$	74	83.6	4.267	28.5	15.5	55.9	0.96	0.99	C_4
Ag_{25}	76	91.4	17.348	6.5	7.8	85.7			
$Ag_{24}Au$	76	92.6	11.721	6.8	7.8	85.4	-0.99	-0.99	
Ag_{25}	77	93.9	23.957	6.3	7.7	86.1			
$Ag_{24}Au$	78	95.9	14.072	9.1	8.3	82.6	0.95	0.79	
Ag_{25}	80	96.3	8.949	10.3	9.3	80.4			
$Ag_{24}Au$	80	97.6	15.063	8.0	8.8	83.3	0.95	0.95	
Ag_{25}	83	101.7	3.005	7.5	6.6	85.9			
$Ag_{24}Au$	85	102.8	1.345	8.5	7.6	84.0	0.87	0.94	
Ag_{25}	84	102.2	4.021	6.6	6.7	86.7			
$Ag_{24}Au$	83	102.1	0.187	4.3	5.1	90.6	-0.74	-0.39	
$Ag_{24}Au$	86	102.9	0.038	5.2	5.3	89.5	0.78	0.67	
Ag_{25}	88	108.4	4.022	6.1	6.0	87.9			
$Ag_{24}Au$	88	109.9	1.629	5.6	5.8	88.6	0.97	0.96	C_5
Ag_{25}	89	111.4	6.790	6.8	6.9	86.3			
$Ag_{24}Au$	90	112.7	5.035	6.1	6.6	87.3	0.95	0.98	
Ag_{25}	91	113.2	3.448	3.4	4.6	92.0			
$Ag_{24}Au$	91	113.5	3.867	3.6	4.7	91.7	0.91	0.94	
Ag_{25}	95	118.8	6.605	3.2	5.4	91.4			
$Ag_{24}Au$	95	119.3	2.005	2.8	6.5	90.7	-0.85	-0.87	
Ag_{25}	96	119.3	12.629	3.1	5.5	91.4			
$Ag_{24}Au$	96	119.4	1.097	2.4	5.6	92.0	0.77	0.68	
Ag_{25}	97	119.5	12.216	3.1	5.9	91.0			
$Ag_{24}Au$	97	120.4	29.900	2.7	6.2	91.1	-0.81	-0.84	
Ag_{25}	100	124.2	1.735	4.2	6.3	89.5			
$Ag_{24}Au$	100	125.4	2.135	4.4	6.2	89.4	0.97	0.98	C_6
Ag_{25}	101	124.9	4.658	3.8	6.1	90.1			
$Ag_{24}Au$	101	126.2	3.348	3.7	5.9	90.4	0.97	0.97	
Ag_{25}	104	127.6	5.646	2.9	5.5	91.6			
$Ag_{24}Au$	104	129.2	3.066	2.5	4.8	92.7	-0.82	-0.86	
$Ag_{24}Au$	105	129.3	3.479	3.5	4.9	91.6	0.37	0.58	
Ag_{25}	105	127.7	5.140	4.3	5.3	90.3			
$Ag_{24}Au$	105	129.3	3.479	3.5	4.9	91.6	-0.86	-0.86	
Ag_{25}	106	130.1	18.532	4.0	6.9	89.1			
$Ag_{24}Au$	106	131.9	34.278	4.4	7.5	88.2	0.93	0.95	

Table S3. (Table S2 continued) Comparison of the nuclear displacement vectors of the Ag_{25} and $Ag_{24}Au$ clusters. Only the modes with significant Raman intensities were considered. All atoms were considered when computing the $O1$ overlap. For $=O2$, the C and H atoms were neglected. Units: Freq (cm^{-1}), Raman (Ang^4/amu).

Figure S12. Raman spectra of [Ag$_{25}$(DMBT)$_{18}$][PPh$_4$] (black trace) and Ag-DMBT thiolates (red trace).

Supporting Information 17
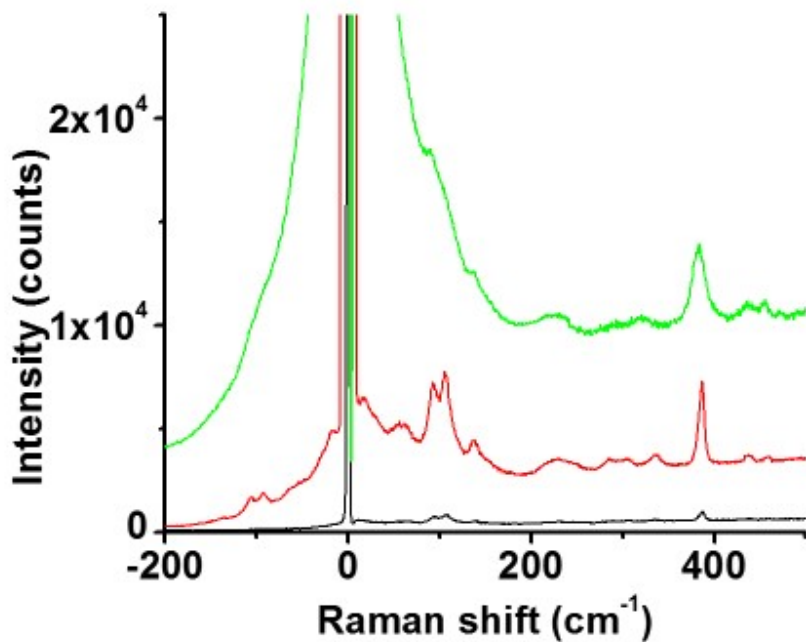
Figure S13. Raman spectra of Ag-DMBT thiolates collected at various lase fluencies (black trace, 0.1 %; red trace, 1 % and green trace, 3.2 %). The low frequency and some of the higher frequency bands disappear as the laser fluency increases.
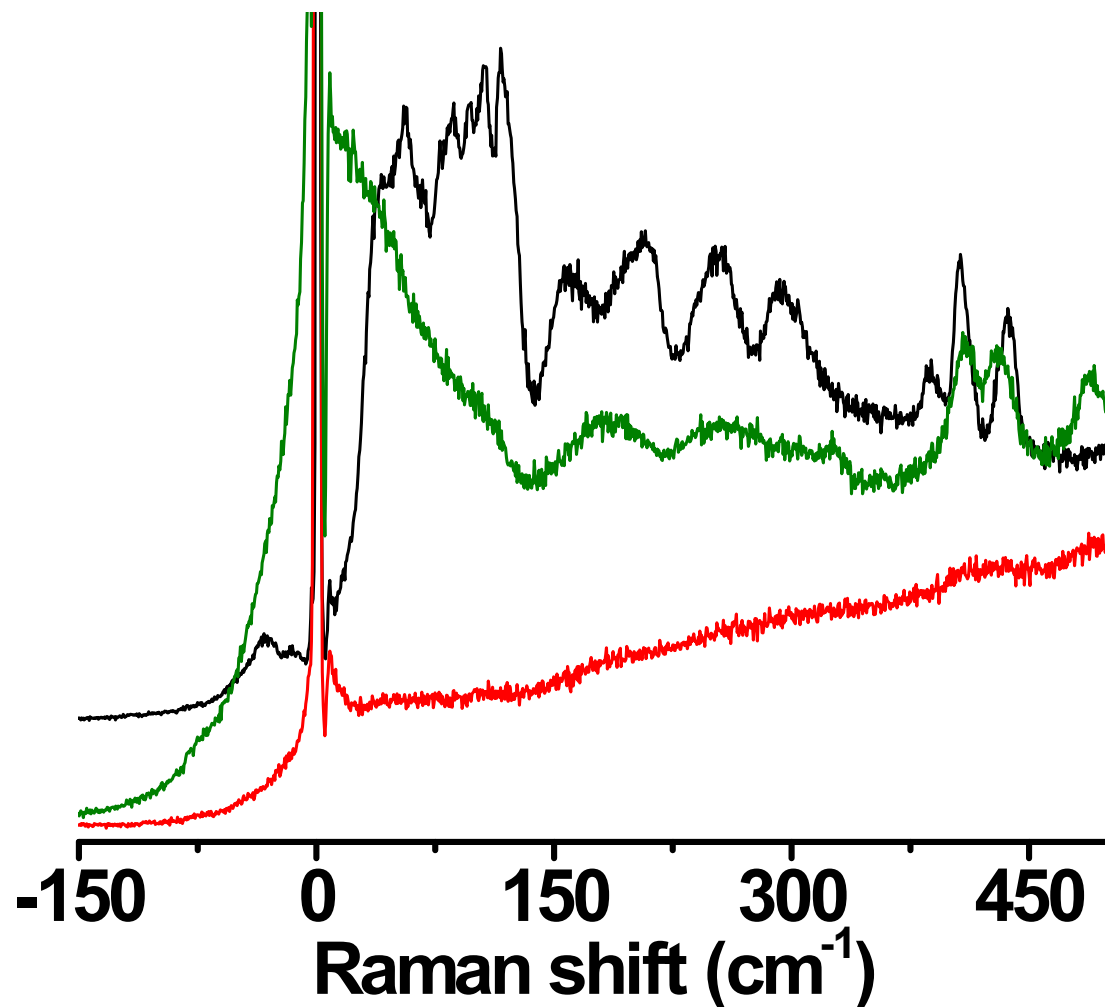
Figure S14. Raman spectra of $[Ag_{29}(BDT)_{12}][Na]_3$ (black trace), Ag-BDT complexes at 0.1 % (red trace) and at 1 % laser fluencies (green trace). It is evident that the spectra of the metal-thiolate complexes are significantly different apart from the overlap of a few higher frequency bands.
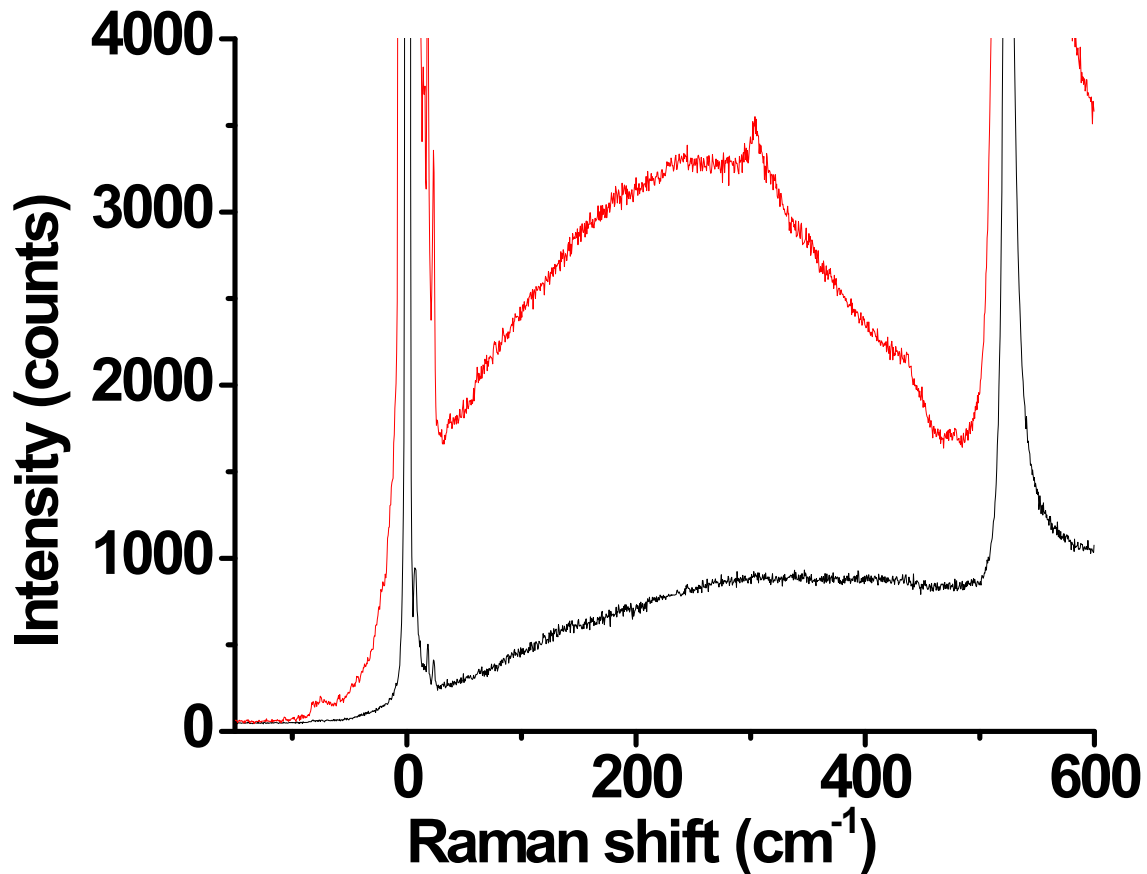
Figure S15. Raman spectra of Au-PET complexes at 0.1 % (black trace) and at 1 % laser fluencies (red trace). The intense band at around 520 cm^{-1} and a weak band at around 320 cm^{-1} are due to the silicon substrate upon which the clusters are drop-casted for Raman measurements. No other bands were observed for the Au-PET thiolate which shows that the spectra of the Au-PET complexes are significantly different from that of $Au_{25}(PET)_{18}$ clusters (see Figure 1 D).

Supporting Information 20

Coordinates of the optimized geometry of $Au_{25}(SCH_3)_{18}$

1	Au	-5.9065	-9.4007	-12.3961
2	Au	-3.8559	-11.3815	-12.4220
3	Au	-3.5888	-8.7815	-13.9353
4	Au	-6.4022	-8.1049	-14.9044
5	Au	-8.2416	-10.0186	-13.8930
6	Au	-6.8235	-12.0983	-12.1882
7	Au	-5.5074	-11.0158	-14.7103
8	Au	-4.6951	-14.0924	-13.9303
9	Au	-2.4111	-11.6578	-15.3407
10	Au	-3.7992	-5.9699	-15.5539
11	Au	-9.4263	-7.3038	-15.4647
12	Au	-7.7712	-10.0458	-17.1106
13	Au	-10.0543	-12.3724	-12.1714
14	Au	-7.9570	-7.4201	-12.3704
15	Au	-8.2240	-10.0199	-10.8567
16	Au	-5.4107	-10.6967	-9.8878
17	Au	-3.5714	-8.7830	-10.8991
18	Au	-4.9895	-6.7032	-12.6041
19	Au	-6.3055	-7.7860	-10.0817
20	Au	-7.1176	-4.7092	-10.8614
21	Au	-9.4019	-7.1439	-9.4514
22	Au	-8.0136	-12.8317	-9.2386
23	Au	-2.3867	-11.4972	-9.3274
24	Au	-4.0419	-8.7553	-7.6815
25	Au	-1.7587	-6.4291	-12.6209

26	S	-1.7876	-9.3904	-15.4732
27	S	-10.3784	-11.1705	-14.1687
28	S	-6.1621	-11.7503	-16.9455
29	S	-9.8864	-13.7735	-10.2938
30	S	-5.6724	-6.6905	-16.7625
31	S	-9.3510	-8.3665	-17.5600
32	S	-9.6864	-6.0827	-13.4719
33	S	-6.4085	-14.4976	-12.3818
34	S	-2.9725	-13.9368	-15.5172
35	S	-10.0261	-9.4112	-9.3198
36	S	-1.4342	-7.6314	-10.6239
37	S	-5.6508	-7.0508	-7.8467
38	S	-1.9265	-5.0281	-14.4986
39	S	-6.1397	-12.1122	-8.0304
40	S	-2.4628	-10.4352	-7.2318
41	S	-2.1262	-12.7183	-11.3202
42	S	-5.4043	-4.3039	-12.4098
43	S	-8.8402	-4.8650	-9.2743
44	C	-11.3058	-13.3503	-9.1950
45	C	-11.5994	-9.5204	-10.2733
46	C	-11.3111	-6.7060	-12.8608
47	C	-10.2427	-3.9585	-10.0580
48	C	-4.0660	-3.5229	-11.4107
49	C	-0.5068	-5.4512	-15.5971
50	C	-0.2136	-9.2802	-14.5210
51	C	-0.8329	-9.5773	-7.1349
52	C	-1.7037	-6.3516	-9.3228
53	C	-6.9611	-7.6276	-6.6827

54	C	-7.7468	-15.2790	-13.3806
55	C	-10.1083	-12.4502	-15.4697
56	C	-10.9807	-9.2250	-17.6560
57	C	-6.7411	-5.1862	-16.7713
58	C	-0.5016	-12.0943	-11.9309
59	C	-1.5699	-14.8427	-14.7329
60	C	-4.8519	-11.1731	-18.1094
61	C	-5.0708	-13.6164	-8.0234
62	H	-11.2240	-13.9744	-8.2973
63	H	-11.2798	-12.2942	-8.9100
64	H	-12.2354	-13.5816	-9.7278
65	H	-11.7875	-10.5807	-10.4861
66	H	-12.4101	-9.1054	-9.6619
67	H	-11.5260	-8.9792	-11.2191
68	H	-11.3699	-6.4963	-11.7846
69	H	-12.1104	-6.1774	-13.3947
70	H	-11.4034	-7.7826	-13.0309
71	H	-10.0009	-2.8894	-10.0319
72	H	-10.3832	-4.2774	-11.0954
73	H	-11.1478	-4.1516	-9.4703
74	H	-3.1580	-3.5090	-12.0253
75	H	-4.3712	-2.4979	-11.1676
76	H	-3.8832	-4.0832	-10.4897
77	H	-0.5886	-4.8271	-16.4949
78	H	0.4226	-5.2197	-15.0641
79	H	-0.5326	-6.5073	-15.8820
80	H	0.5968	-9.6949	-15.1331
81	H	-0.0258	-8.2197	-14.3086

82	H	-0.2858	-9.8212	-13.5751
83	H	-0.0593	-10.3420	-6.9970
84	H	-0.6331	-9.0105	-8.0499
85	H	-0.8538	-8.9070	-6.2676
86	H	-1.8159	-6.8706	-8.3622
87	H	-0.8337	-5.6845	-9.2998
88	H	-2.6147	-5.7805	-9.5219
89	H	-6.5902	-7.5060	-5.6580
90	H	-7.8444	-6.9973	-6.8434
91	H	-7.2183	-8.6743	-6.8682
92	H	-7.4415	-16.3039	-13.6236
93	H	-8.6548	-15.2929	-12.7659
94	H	-7.9299	-14.7189	-14.3017
95	H	-10.9781	-13.1177	-15.4928
96	H	-9.9961	-11.9312	-16.4303
97	H	-9.1972	-13.0210	-15.2705
98	H	-11.7546	-8.4605	-17.7936
99	H	-10.9601	-9.8954	-18.5231
100	H	-11.1798	-9.7917	-16.7407
101	H	-6.2950	-4.4528	-17.4539
102	H	-7.7325	-5.4861	-17.1328
103	H	-6.8289	-4.7609	-15.7677
104	H	0.2978	-12.6225	-11.3968
105	H	-0.4424	-12.3040	-13.0071
106	H	-0.4099	-11.0176	-11.7607
107	H	-1.4297	-14.5232	-13.6955
108	H	-1.8115	-15.9118	-14.7584
109	H	-0.6648	-14.6497	-15.3205

110 H	-3.9685	-11.8033	-17.9486
111 H	-5.2227	-11.2947	-19.1341
112 H	-4.5949	-10.1263	-17.9237
113 H	-4.0792	-13.3165	-7.6625
114 H	-5.5163	-14.3502	-7.3409
115 H	-4.9838	-14.0411	-9.0273

Coordinates of the optimized geometry of $Ag_{25}(SCH_3)_{18}$

1 Ag	-5.9064	-9.4008	-12.3960
2 Ag	-3.8464	-11.3479	-12.3940
3 Ag	-3.5887	-8.8014	-13.9133
4 Ag	-6.3317	-8.0849	-14.8694
5 Ag	-8.2376	-10.0282	-13.8735
6 Ag	-6.7566	-12.0978	-12.2407
7 Ag	-5.5401	-10.9598	-14.7263
8 Ag	-4.7376	-13.8575	-13.9235
9 Ag	-2.5377	-11.4601	-15.2358
10 Ag	-3.9173	-6.1076	-15.3813
11 Ag	-9.2387	-7.3326	-15.2833
12 Ag	-7.6902	-9.9611	-16.9254
13 Ag	-9.8450	-12.2633	-12.2212
14 Ag	-7.9668	-7.4540	-12.3979
15 Ag	-8.2243	-10.0001	-10.8790
16 Ag	-5.4815	-10.7163	-9.9225
17 Ag	-3.5747	-8.7734	-10.9192
18 Ag	-5.0560	-6.7038	-12.5514
19 Ag	-6.2726	-7.8416	-10.0659
20 Ag	-7.0752	-4.9442	-10.8682

21	Ag	-9.2754	-7.3419	-9.5562
22	Ag	-7.8957	-12.6937	-9.4108
23	Ag	-2.5743	-11.4687	-9.5091
24	Ag	-4.1222	-8.8398	-7.8672
25	Ag	-1.9677	-6.5382	-12.5714
26	S	-1.6434	-9.2188	-15.4604
27	S	-10.4603	-11.1295	-14.2698
28	S	-6.2158	-11.8736	-16.9597
29	S	-9.7883	-13.8332	-10.3911
30	S	-5.6450	-6.8035	-16.9173
31	S	-9.3079	-8.2684	-17.5085
32	S	-9.7349	-5.9399	-13.3636
33	S	-6.4014	-14.5809	-12.3327
34	S	-3.0214	-13.7943	-15.6211
35	S	-10.1697	-9.5831	-9.3319
36	S	-1.3520	-7.6721	-10.5230
37	S	-5.5961	-6.9269	-7.8331
38	S	-2.0244	-4.9683	-14.4015
39	S	-6.1683	-11.9975	-7.8746
40	S	-2.5049	-10.5328	-7.2839
41	S	-2.0782	-12.8620	-11.4285
42	S	-5.4113	-4.2207	-12.4589
43	S	-8.7917	-5.0076	-9.1709
44	C	-11.1893	-13.3523	-9.2898
45	C	-11.6884	-9.5979	-10.3822
46	C	-11.3843	-6.5947	-12.8487
47	C	-10.1919	-4.0955	-9.9553
48	C	-4.0966	-3.4521	-11.4126

49	C	-0.6237	-5.4494	-15.5030
50	C	-0.1247	-9.2039	-14.4102
51	C	-0.8701	-9.6771	-7.2495
52	C	-1.6243	-6.3639	-9.2458
53	C	-6.8837	-7.4211	-6.6011
54	C	-7.7161	-15.3498	-13.3789
55	C	-10.1879	-12.4378	-15.5469
56	C	-10.9425	-9.1245	-17.5430
57	C	-6.7061	-5.2953	-17.0572
58	C	-0.4288	-12.2070	-11.9438
59	C	-1.6212	-14.7065	-14.8369
60	C	-4.9280	-11.3786	-18.1910
61	C	-5.1071	-13.5055	-7.7343
62	H	-11.1383	-13.9738	-8.3875
63	H	-11.1172	-12.2965	-9.0033
64	H	-12.1362	-13.5403	-9.8098
65	H	-11.9963	-10.6409	-10.5288
66	H	-12.4863	-9.0522	-9.8638
67	H	-11.5088	-9.1442	-11.3607
68	H	-11.5232	-6.4080	-11.7762
69	H	-12.1608	-6.0652	-13.4146
70	H	-11.4694	-7.6687	-13.0409
71	H	-9.9828	-3.0217	-9.8767
72	H	-10.2913	-4.3661	-11.0132
73	H	-11.1179	-4.3276	-9.4156
74	H	-3.1865	-3.3659	-12.0182
75	H	-4.4323	-2.4532	-11.1084
76	H	-3.8891	-4.0513	-10.5208

77	H	-0.6748	-4.8280	-16.4054
78	H	0.3234	-5.2616	-14.9832
79	H	-0.6959	-6.5053	-15.7895
80	H	0.6731	-9.7498	-14.9285
81	H	0.1834	-8.1608	-14.2640
82	H	-0.3043	-9.6573	-13.4316
83	H	-0.0850	-10.4348	-7.1375
84	H	-0.7015	-9.1125	-8.1746
85	H	-0.8482	-8.9996	-6.3873
86	H	-1.5615	-6.8308	-8.2550
87	H	-0.8419	-5.6020	-9.3433
88	H	-2.6094	-5.8992	-9.3512
89	H	-6.4544	-7.3416	-5.5952
90	H	-7.7265	-6.7263	-6.6979
91	H	-7.2307	-8.4450	-6.7706
92	H	-7.3803	-16.3486	-13.6831
93	H	-8.6262	-15.4360	-12.7733
94	H	-7.9237	-14.7506	-14.2708
95	H	-10.9704	-13.1996	-15.4495
96	H	-10.2504	-11.9710	-16.5377
97	H	-9.2029	-12.9026	-15.4413
98	H	-11.7277	-8.3669	-17.6549
99	H	-10.9642	-9.8019	-18.4052
100	H	-11.1110	-9.6892	-16.6179
101	H	-6.1919	-4.5662	-17.6951
102	H	-7.6540	-5.5883	-17.5241
103	H	-6.9026	-4.8490	-16.0777
104	H	0.3477	-12.7365	-11.3781

105	H	-0.2902	-12.3937	-13.0164
106	H	-0.3438	-11.1330	-11.7516
107	H	-1.5217	-14.4359	-13.7790
108	H	-1.8303	-15.7803	-14.9155
109	H	-0.6952	-14.4744	-15.3766
110	H	-4.0851	-12.0733	-18.0944
111	H	-5.3570	-11.4577	-19.1971
112	H	-4.5812	-10.3547	-18.0211
113	H	-4.1593	-13.2123	-7.2673
114	H	-5.6213	-14.2346	-7.0965
115	H	-4.9104	-13.9519	-8.7138

Coordinates of the optimized geometry of $Ag_{24}Au1(SCH_3)_{18}$

1	Au	-5.9064	-9.4007	-12.3961
2	Ag	-3.8425	-11.3481	-12.3834
3	Ag	-3.5889	-8.8126	-13.9223
4	Ag	-6.3265	-8.0807	-14.8751
5	Ag	-8.2429	-10.0415	-13.8648
6	Ag	-6.7466	-12.1045	-12.2391
7	Ag	-5.5502	-10.9601	-14.7343
8	Ag	-4.7409	-13.8682	-13.9149
9	Ag	-2.5333	-11.4622	-15.2359
10	Ag	-3.9193	-6.1125	-15.3968
11	Ag	-9.2476	-7.3300	-15.2783
12	Ag	-9.8462	-12.2658	-12.2219

14	Ag	-7.9704	-7.4536	-12.4087
15	Ag	-8.2238	-9.9887	-10.8699
16	Ag	-5.4864	-10.7206	-9.9170
17	Ag	-3.5696	-8.7601	-10.9277
18	Ag	-5.0662	-6.6969	-12.5531
19	Ag	-6.2624	-7.8413	-10.0579
20	Ag	-7.0718	-4.9333	-10.8771
21	Ag	-9.2796	-7.3394	-9.5562
22	Ag	-7.8936	-12.6887	-9.3954
23	Ag	-2.5652	-11.4714	-9.5140
24	Ag	-4.1264	-8.8304	-7.8631
25	Ag	-1.9666	-6.5356	-12.5705
26	S	-1.6411	-9.2179	-15.4529
27	S	-10.4542	-11.1378	-14.2778
28	S	-6.1959	-11.8730	-16.9670
29	S	-9.7854	-13.8239	-10.3817
30	S	-5.6578	-6.8077	-16.9233
31	S	-9.3092	-8.2781	-17.4985
32	S	-9.7269	-5.9312	-13.3568
33	S	-6.4069	-14.5812	-12.3192
34	S	-3.0316	-13.7942	-15.6192
35	S	-10.1717	-9.5837	-9.3393
36	S	-1.3584	-7.6635	-10.5146
37	S	-5.6167	-6.9282	-7.8253
38	S	-2.0272	-4.9774	-14.4107
39	S	-6.1551	-11.9934	-7.8688
40	S	-2.5034	-10.5232	-7.2939
41	S	-2.0859	-12.8705	-11.4355

42	S	-5.4059	-4.2203	-12.4728
43	S	-8.7812	-5.0074	-9.1729
44	C	-11.1915	-13.3471	-9.2853
45	C	-11.6782	-9.6077	-10.4067
46	C	-11.3773	-6.5709	-12.8263
47	C	-10.1836	-4.0835	-9.9396
48	C	-4.0864	-3.4498	-11.4339
49	C	-0.6214	-5.4546	-15.5072
50	C	-0.1346	-9.1939	-14.3856
51	C	-0.8693	-9.6668	-7.2541
52	C	-1.6463	-6.3565	-9.2396
53	C	-6.9076	-7.4425	-6.6052
54	C	-7.7263	-15.3517	-13.3581
55	C	-10.1665	-12.4449	-15.5528
56	C	-10.9433	-9.1346	-17.5384
57	C	-6.7181	-5.2986	-17.0588
58	C	-0.4355	-12.2307	-11.9662
59	C	-1.6293	-14.7181	-14.8526
60	C	-4.9048	-11.3588	-18.1870
61	C	-5.0948	-13.5025	-7.7331
62	H	-11.1400	-13.9662	-8.3814
63	H	-11.1255	-12.2902	-9.0011
64	H	-12.1360	-13.5410	-9.8075
65	H	-11.9645	-10.6533	-10.5775
66	H	-12.4916	-9.0874	-9.8860
67	H	-11.4969	-9.1311	-11.3738
68	H	-11.4980	-6.3979	-11.7491
69	H	-12.1538	-6.0221	-13.3733

70	H	-11.4804	-7.6406	-13.0327
71	H	-9.9692	-3.0113	-9.8543
72	H	-10.2928	-4.3454	-10.9985
73	H	-11.1064	-4.3156	-9.3944
74	H	-3.1768	-3.3714	-12.0413
75	H	-4.4184	-2.4476	-11.1369
76	H	-3.8803	-4.0432	-10.5379
77	H	-0.6729	-4.8355	-16.4111
78	H	0.3233	-5.2606	-14.9851
79	H	-0.6875	-6.5114	-15.7912
80	H	0.6787	-9.7144	-14.9062
81	H	0.1518	-8.1483	-14.2150
82	H	-0.3159	-9.6703	-13.4184
83	H	-0.0839	-10.4245	-7.1442
84	H	-0.7000	-9.0983	-8.1767
85	H	-0.8490	-8.9931	-6.3890
86	H	-1.6047	-6.8254	-8.2486
87	H	-0.8574	-5.5995	-9.3219
88	H	-2.6262	-5.8852	-9.3622
89	H	-6.4857	-7.3629	-5.5962
90	H	-7.7574	-6.7565	-6.7043
91	H	-7.2419	-8.4695	-6.7815
92	H	-7.3944	-16.3539	-13.6552
93	H	-8.6359	-15.4301	-12.7508
94	H	-7.9324	-14.7583	-14.2542
95	H	-10.9556	-13.2018	-15.4705
96	H	-10.2080	-11.9760	-16.5438
97	H	-9.1867	-12.9164	-15.4302

98	H	-11.7288	-8.3769	-17.6483
99	H	-10.9635	-9.8083	-18.4035
100	H	-11.1126	-9.7031	-16.6158
101	H	-6.2081	-4.5733	-17.7044
102	H	-7.6708	-5.5916	-17.5160
103	H	-6.9043	-4.8481	-16.0793
104	H	0.3410	-12.7795	-11.4193
105	H	-0.3151	-12.4037	-13.0433
106	H	-0.3324	-11.1610	-11.7597
107	H	-1.5201	-14.4563	-13.7936
108	H	-1.8437	-15.7903	-14.9379
109	H	-0.7065	-14.4860	-15.3978
110	H	-4.0552	-12.0450	-18.0880
111	H	-5.3268	-11.4384	-19.1961
112	H	-4.5705	-10.3319	-18.0107
113	H	-4.1421	-13.2094	-7.2759
114	H	-5.6048	-14.2278	-7.0875
115	H	-4.9085	-13.9531	-8.7126